JACS
JOURNAL OF THE AMERICAN CHEMICAL SOCIETY
Article
pubs.acs.org/JACS

DNA Scaffolds for the Dictated Assembly of Left-/Right-Handed Plasmonic Au NP Helices with Programmed Chiro-Optical Properties

Alessandro Cecconello,[†] Jason S. Kahn,[†] Chun-Hua Lu,[†] Larousse Khosravi Khorashad,[‡] Alexander O. Govorov,[‡] and Itamar Willner*[,†]

[†]The Institute of Chemistry, The Center for Nanoscience and Nanotechnology, The Hebrew University of Jerusalem, Jerusalem 91904, Israel

[‡]Department of Physics and Astronomy, Ohio University, Athens, Ohio 45701, United States

Supporting Information

ABSTRACT: Within the broad interest of assembling chiral left- and right-handed helices of plasmonic nanoparticles (NPs), we introduce the DNA-guided organization of left- or right-handed plasmonic Au NPs on DNA scaffolds. The method involves the self-assembly of stacked 12 DNA quasi-rings interlinked by 30 staple-strands. By the functionalization of one group of staple units with programmed tether-nucleic acid strands and additional staple elements with long nucleic acid chains, acting as promoter strands, the promoter-guided assembly of barrels modified with 12 left- or right-handed tethers is achieved. The subsequent hybridization of Au NPs functionalized with single nucleic acid tethers yields left- or right-handed structures of plasmonic NPs. The plasmonic NP structures reveal CD spectra at the plasmon absorbance, and the NPs are imaged by HR-TEM. Using geometrical considerations corresponding to the left- and right-handed helices of the Au NPs, the experimental CD spectra of the plasmonic Au NPs are modeled by theoretical calculations.

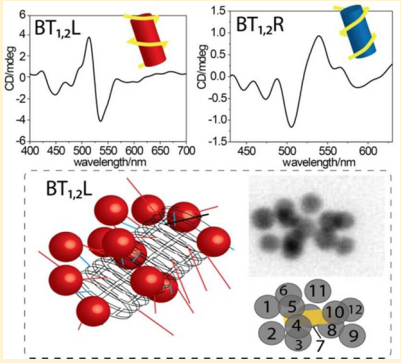

INTRODUCTION

Chirality at the nanometer scale has recently attracted substantial experimental and theoretical research efforts aimed to mimic biological systems and to develop new bioinspired materials.[1−4] Specifically, chirality involving nanomaterials is a rapidly progressing field that includes many experimental and theoretical challenges.[5−8] Different mechanistic paradigms to assemble chiral nanostructures have been reported. By one approach, nanoparticles (NPs),[9−12] nanotubes,[13,14] or nanorods[15,16] are functionalized with chiral ligands, resulting in electronic coupling between the electronic states of the nanomaterials and the ligands in the hybrid structures.[17,18] This leads to ligand-induced chiral properties of the nanomaterial core.[19,20] By a second approach, enantioselective synthesis of inorganic NPs, such as SiO_2,[21−23] TiO_2,[24] or asymmetrically shaped plasmonic Au NPs,[25] yields chiral nanostructures. A third paradigm to assemble chiral nanostructures includes the use of different sized, different shaped, or different constitutional compositions of achiral nanomaterials for their programmed deposition on chiral scaffolds, such as peptides.[26,27] Specifically, the information encoded in the base-sequence of duplex DNA structures provides versatile rules to assemble chiral-configurational structures of nanomaterials.[28,29] The DNA-guided assembly of four-different-sized Au NPs bridged by duplex DNA has been suggested to yield chiral Au NP aggregates,[30] and the anchoring of different nanoparticle constituents (Au NPs, Ag NPs, NC-QDs) on the corners of DNA pyramid scaffolds has provided effective means to construct chiral plasmonic nanostructures.[31] Progress in designing origami frames with programmed protruding nucleic acid tethers[32−34] enabled the tailored anchoring of chiral nanostructures on the origami scaffold. For example, Au NPs were hybridized with left- or right-handed configurations of nucleic acid tethers associated with DNA origami bundles, to yield left- or right-handed helical assemblies of Au NPs that revealed chiro-optical properties.[35] Similarly, asymmetric deposition of Au NPs[36] or Au nanorods[37] on origami scaffolds led to the formation of chiral structures exhibiting chiral plasmonic functions. Also, the reconfiguration of chiral Au NP assemblies on structurally switchable origami-bundle scaffolds led to switchable chiral plasmonic properties of the structures in solution[38] or on surfaces.[39] Different applications of chiro-plasmonic nanostructures were discussed, including their use in imaging mechanical functions of nanoscale machines,[40] their applications as sensors,[41] and their possible use as waveguides.[42,43]

In contrast to previous reports that implemented origami scaffolds to organize the chiral structures of the plasmonic nanoparticles, we introduce self-assembled DNA barrels modified with right- or left-handed helical configurations of tethers that act as scaffolds for the anchoring of right- or left-handed chiral Au NP structures on the barrels. In contrast to previous reports that required the predesign of two mirror images of chiral tethering sites on DNA scaffolds, we introduce a new paradigm, where steric and electrostatic interactions

Received: May 9, 2016
Published: July 18, 2016

DOI: 10.1021/jacs.6b04096
J. Am. Chem. Soc. 2016, 138, 9895−9901

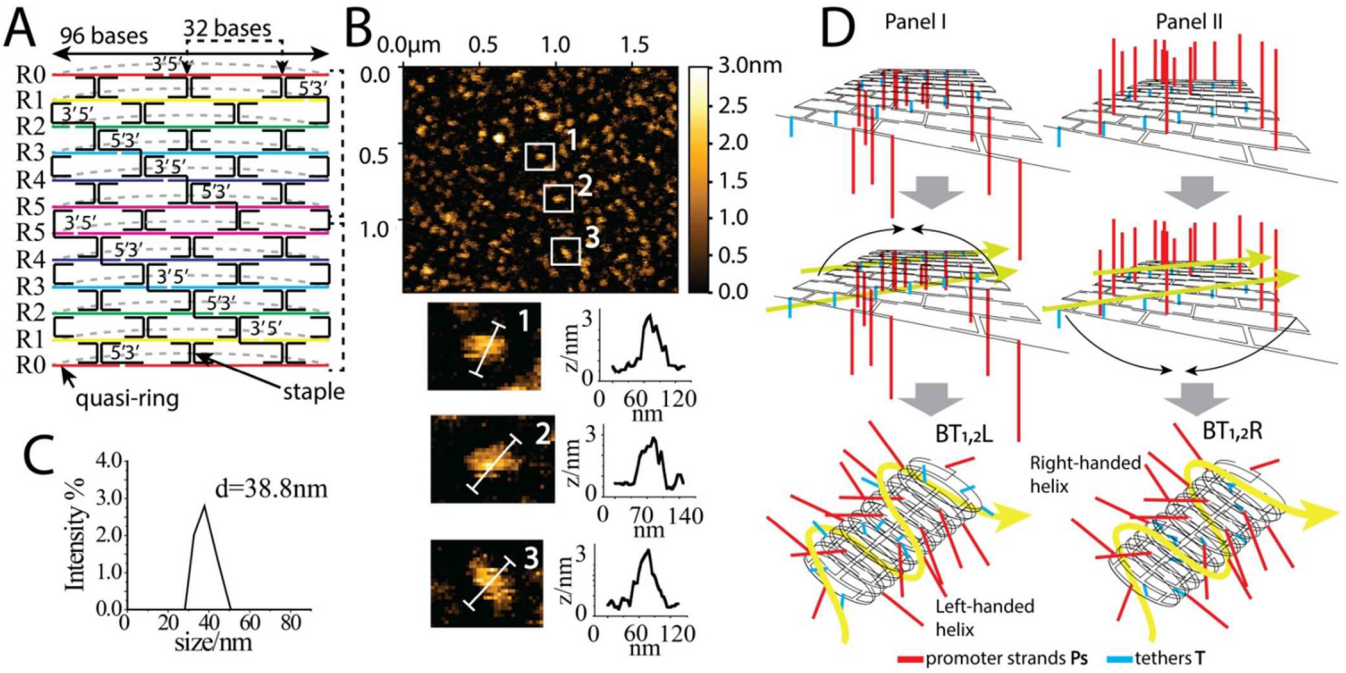

Figure 1. (A) Schematics of the DNA barrels composed of quasi-circles of nucleic acids R0, R1, R2, R3, R4, and R5, stapled by short strands that form crossover DNA junctions between consecutive quasi-circles. (B) AFM images of the DNA nanobarrels and accompanying cross-section analysis of three nanostructures (images recorded in liquid). (C) Dynamic light scattering results corresponding to the average hydrodynamic diameter of the DNA barrel. (D) Schematic presentation of the self-assembly of the DNA barrels functionalized with left-handed, Panel I, or right-handed configuration, Panel II, of the anchoring tethers, T. In Panel I, the promoting strands, Ps (colored in red), associated with the respective staples and the tether strands, T (colored in blue), associated with the respective staple units, are beyond the "imaginary" surface of the quasi circle units forming the barrels. The electrostatic/steric-dictated folding of the quasi-circle-based barrels leads to the left-handed configuration of the anchoring tethers, T, $BT_{1,2}L$. In Panel II, the promoter strands, Ps, associated with the respective staples, and the tether strands, T, associated with the respective staple units, are above the "imaginary" surface of the quasi-circle units forming the barrels. The electrostatic/steric-dictated folding of the quasi-circle-based barrels leads to the right-handed configuration of the anchoring tethers T, $BT_{1,2}R$. (For the assembly of the mirror images of the chiral barrels $BT_{3,4}L$ and $BT_{3,4}R$, see Figure S2.)

introduced by auxiliary nucleic acid promoter strands drive the dictated assembly of right/left helical configurations of functionalized tethers for the attachment of the NPs.

The CD signals from the right-handed and left-handed helices are indeed inverted, as expected, yet they have remarkably different amplitudes. We rationalized this observation in terms of a global right-hand twist in the structure of the barrels, originating from an unbalanced number of base-pairs per turn in the duplexes comprising the barrels that leads to nonexact mirror images of the two Au NP helices.

This study advances the area of chiroplasmonic nanoparticle structures by introducing new methods to assemble the systems and by addressing important phenomena controlling their properties. Besides the basic significance of the results, we believe that the scalability of the barrel structure into nanowire architectures, followed by the helical immobilization of Au NPs, could lead, in the future, to chiroplasmonic wave-guides.

RESULTS AND DISCUSSION

The method for the assembly of the DNA barrel construct is depicted in Figure 1A. The method is based on the recently reported method for the construction of DNA nanotubes by the self-assembly of circular DNAs by means of crossover junctions acting as stapling motifs between the stacked rings.[44] By our approach we use a mixture of 6 long single strands R_0, R_1, R_2, R_3, R_4 R_5, each consisting of 96 bases, and 30 short oligonucleotides acting as capping units and staples (6 caps and 24 staples). For the full detailed list of DNA sequences, see the Supporting Information. The capping units hybridize with each of the six R strands to yield a quasi-circular structure. The staple units include appropriate base sequences to form crossover junctions between neighboring quasi-rings to yield rigidified barrels composed of 12 quasi-rings stacked in a programmed configuration $R_0 \rightarrow R_1 \rightarrow R_2 \rightarrow R_3 \rightarrow R_4 \rightarrow R_5 \rightarrow R_5 \rightarrow R_4 \rightarrow R_3 \rightarrow R_2 \rightarrow R_1 \rightarrow R_0$ (tail-to-tail stacking). Figure 1A depicts schematically the 2D projection of the barrel structure "cut" along the longitudinal direction of the barrel. We should note, however, that in contrast to the previously reported method to construct DNA nanotubes of undefined length, via the linkage of circular DNAs by crossover forming staples, our approach leads to defined barrel structures of 12 quasi-rings. The resulting barrel dimensions were evaluated by AFM imaging, Figure 1B, and by Dynamic light scattering (DLS) experiments that indicated that only upon mixing of all components, we generate supramolecular structures with a hydrodynamic average diameter corresponding to ca. 39 nm, consistent with the design of the barrels, Figure 1C. Furthermore, by designing staple units that allow the limitless head-to-tail assembly of the quasi-rings, the self-assembly of the R_0–R_5 into long nanotubes was demonstrated (for a detailed discussion and AFM images, see Supporting Information, Figure S1 and accompanying description).

Figure 1D depicts the method to dictate the assembly of the chiral helical structures of nucleic acid tethers on the DNA barrels. In this process, we further modify the constituents of the rings/staple units comprising the barrels by the addition of

DOI: 10.1021/jacs.6b04096
J. Am. Chem. Soc. 2016, 138, 9895–9901

several elements: (i) We conjugate to the appropriate staple units the sequences (blue) acting as tethers, T (these tethers will be used as anchoring sites for the hybridization of T′-modified Au NPs, vide infra). The tethers T are linked to the appropriate staples to form, upon assembly of the barrels, right- or left-handed helices of the tethers, as desired. (ii) To other staple units, long nucleic acids (red) composed of identical base-sequences are conjugated. These sequences are aimed to act as promoter strands, Ps, that introduce electrostatic repulsive interactions and/or steric perturbing interactions upon the wrapping and self-assembly of the barrels. That is, the promoter units Ps dictate the assembly of the stacked quasi-ring by minimizing the energy of the resulting barrel via retaining the promoter units in a perpendicular orientation to the exterior surface of the barrels (rather than to the inner surface), originating from a constant eight-base distance at the promoters from the crossover junctions. Accordingly, the dictated assembly of the barrels by the promoter strands leads to the left-handed tether configuration $BT_{1,2}L$ or right-handed configuration of the tethers $BT_{1,2}R$. Note that the barrels $BT_{1,2}L$ and $BT_{1,2}R$ include two tether sequences T_1 and T_2, attached to the staple units, that functionalize the barrels. The left-handed (L) or right-handed (R) configurations are dictated by the promoter strands.

It should be noted that a further permutation of the tether sequences T, associated with the appropriate staples allows, in the presence of the quasi-circles R_0–R_5 and the promoter-modified staples outlined in Figure 1D, panel I and panel II, the assembly of barrels that include opposite chiralities of the tethers decorating the barrels. Barrels $BT_{3,4}R$ and $BT_{3,4}L$ are counter structures of $BT_{1,2}L$ and $BT_{1,2}R$, respectively. It is relevant to note that the majority of the staple units in the different barrels have identical sequences and only the staples needed for joining the two R5 quasi-rings differ for geometrical reasons (for a detailed discussion of the formation of $BT_{3,4}R$ and $BT_{3,4}L$, see Supporting Information, Figure S2 and accompanying discussion). It should be noted, however, that in the barrels $BT_{3,4}R$ and $BT_{3,4}L$ the tethers T_3 and T_4 are identical in their sequences to T_1 and T_2, respectively, but they are attached to mirror-image staple units associated with the barrels $BT_{1,2}L$ and $BT_{1,2}R$, respectively.

In the next step, Au NPs, 10 nm diameter, functionalized with a single nucleic acid T_1' or T_2', complementary to the tethers T_1 and T_2 associated with the barrels $BT_{1,2}L$ and $BT_{1,2}R$ (or complementary to tethers T_3 and T_4 associated with the barrels $BT_{3,4}L$ or $BT_{3,4}R$), were hybridized with the respective barrels to yield the chiral structures of 12 Au NPs on the respective barrel scaffolds. The modification of the Au NPs with a single nucleic acid complementary to the tether units is important to prevent the aggregation of the nanoparticle-modified barrels (for the synthesis and separation of the single nucleic acid-functionalized Au NPs, see Figure S3 and associated discussion).

The hybridization of the T_1'- and T_2'-modified Au NPs on the barrels $BT_{1,2}L$ or $BT_{1,2}R$ yielded the left (L)-handed or right (R)-handed assemblies of the Au NPs (similarly, the hybridization of T_3'- and T_4'-modified Au NPs to the $BT_{3,4}R$ and $BT_{3,4}L$ barrels yields the respective (R)-handed or (L)-handed assemblies of the Au NPs). Figure 2A depicts schematically the assembly of the (L)-handed assembly of the Au NPs on the barrels $BT_{1,2}L$ (for the similar assembly of the (R)-handed structure of the Au NPs on the $BT_{1,2}R$, see Supporting Information, Figure S4). Figure 2B exemplifies the

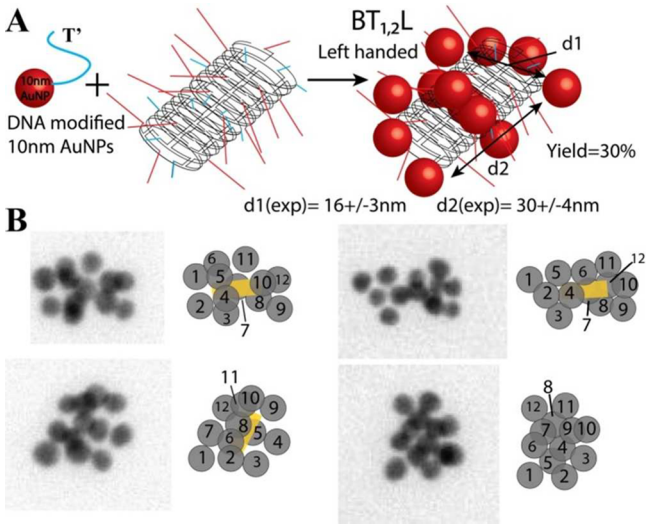

Figure 2. (A) Schematic anchoring of nucleic acid functionalized Au NPs (10 nm) to the left-handed configuration of the tethers associated with the barrels $BT_{1,2}L$ to yield the left-handed configuration of 12 Au NPs (for a similar assembly of the right-handed configuration of 12 Au NPs, see Figure S4). (B) Representative TEM images of the left-handed 12 Au NPs helical structure and schematic models of the Au NPs decorating the barrels. The distances separating Au NPs on opposite sides and end-Au NPs, d_1 and d_2, were estimated from the TEM images and are provided in the schematic left-handed structure in (A). For TEM images of the right- or left-handed helical structures associated with barrels $BT_{1,2}R$, $BT_{3,4}R$, $BT_{3,4}L$, and the respective derived distances, see Figures S4, S6, and S7.

HR-TEM image of the 12 Au NPs structures associated with the barrels $BT_{1,2}L$ (on the right of each of these (L)-handed Au NPs helices, schematic models of the Au NPs linked to the tethers T_1 and T_2 are marked). From the HR-TEM images we estimate the maximum spatial separation between two Au NPs, on opposite sides of the barrel to be $d_1 = 16 \pm 3$ nm and the distance separating two Au NPs at the ends of the barrel to be $d_2 = 30 \pm 4$ nm. These values are consistent with the calculated dimensions of the width/length of the barrels and taking into account the length of the tethers and the dimensions of the NPs. Figure S4, in the Supporting Information, similarly, shows examples for the HR-TEM images of the 12 Au NP structures associated with the mirror image barrels $BT_{1,2}R$. Also, a discussion relating the two-dimensional HR-TEM images of the 12 Au NP structures associated with $BT_{1,2}L$ and $BT_{1,2}R$, and the two-dimensional projection of the 3D-model of the left- and right-handed helical structures of the NPs is provided in Figure S5. Furthermore, Figures S6 and S7, Supporting Information, provide the HR-TEM images of the 12 Au NPs associated with the chiral structures $BT_{3,4}R$ and $BT_{3,4}L$; while Figures S8–S11 show examples of large area HR-TEM images of the respective structures. The yield of the purified Au NP $BT_{1,2}L$ structures is estimated to be ca. 30% and representative HR-TEM images are presented in Figure S8. While most of the structures include the expected 12 Au NPs, some of the structures show defects, where only 10 or 11 particles comprise the helical structures. It should be noted that most of the barrels are functionalized with 12 nanoparticles, while some of the barrels include defects where the helices include 10 and 11 nanoparticles (a trace of barrels included 13 nanoparticles, presumably due to nonspecific adsorption to the barrels); see histograms of the composition of the barrels, Figure S12.

DOI: 10.1021/jacs.6b04096
J. Am. Chem. Soc. 2016, 138, 9895–9901

Furthermore, attempts to further purify the intact 12-nanoparticle-modified barrels by electrophoresis were unsuccessful due to partial dissociation of the NPs from the barrel structures during electrophoresis and extraction of the products from the gel.

Figure 3A and B depicts the CD spectra corresponding to the (L)-handed and (R)-handed helical structures of the 12 NPs

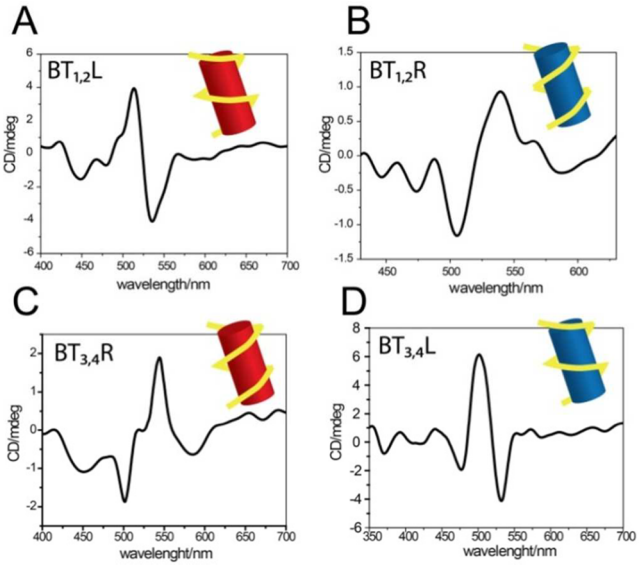

Figure 3. CD spectra corresponding to (A) the helical left-handed structure and associated with the barrel $BT_{1,2}L$; (B) the helical right-handed structure associated with the barrel $BT_{1,2}R$; (C) the helical right-handed structure associated with barrel $BT_{3,4}R$; (D) the helical left-handed structure associated with barrel $BT_{3,4}L$.

associated with the $BT_{1,2}L$ and $BT_{1,2}R$ barrels, respectively. Similarly, Figure 3C and D shows the CD spectra of the (R)-handed and (L)-handed helical structures of the 12 Au NPs associated with the $BT_{3,4}R$ and $BT_{3,4}L$, respectively. As expected, the CD spectra show characteristic bisignate peak/dip bands centered around the plasmon absorbance band of the Au NPs. Also, the CD spectra show mirror images of the (L)- and (R)-handed assemblies. The clear CD spectra originate from the fact that the effective interparticle plasmonic coupling occurs in the helical structures of the Au NPs, positioned at close spatial distances on the respective barrels. Accordingly, increased absorbance of the incident light proceeds along the respective helical structures of the Au NPs possessing the same helicity of the circularly polarized light. It should be noted that although some "shoulders" appear on the central CD bands, these perturbations of the CD bands may be attributed to the existence of defective, imperfect structures of the Au NPs (resulting in larger interparticle distances) and/or the heterogeneity of the 10 nm-sized Au NPs. The absorbance spectra of the different helical Au NP structures associated with the barrels $BT_{1,2}L$, $BT_{1,2}R$, $BT_{3,4}R$, and $BT_{3,4}L$ are depicted in Figure S13A, and the calculated extinction Discrete Dipole Approximation (DDA) spectrum of $BT_{1,2}R$, used to simulate the CD spectra, is depicted in Figure S13B. From the respective CD spectra and absorption spectra of the structures, the anisotropy *g*-factors of the systems were calculated to be 0.6×10^{-2}, 0.1×10^{-2}, 0.5×10^{-2}, and 0.6×10^{-2} (at the respective CD band peaks of barrels $BT_{1,2}L$, $BT_{1,2}R$, $BT_{3,4}R$, and $BT_{3,4}L$), Figure S14, consistent with previously reported g-factors for other chiral Au NPs structures.[31,41,45] Furthermore, we note that the CD spectra associated with the left-handed Au NP assemblies are always 2.5- to 3-fold enhanced as compared to the right-handed Au NPs assemblies (this conclusion is derived from a set of $N = 5$ experiments). The experimental data fit well the theoretical calculations, taking into account the absorbance of the circularly polarized light from the chiro-plasmonic NP structures.[46−48] For these calculations we adopted the geometrical model of the Au NPs as depicted in Figure 4A. From the HR-TEM images, we conclude that the spatial separation

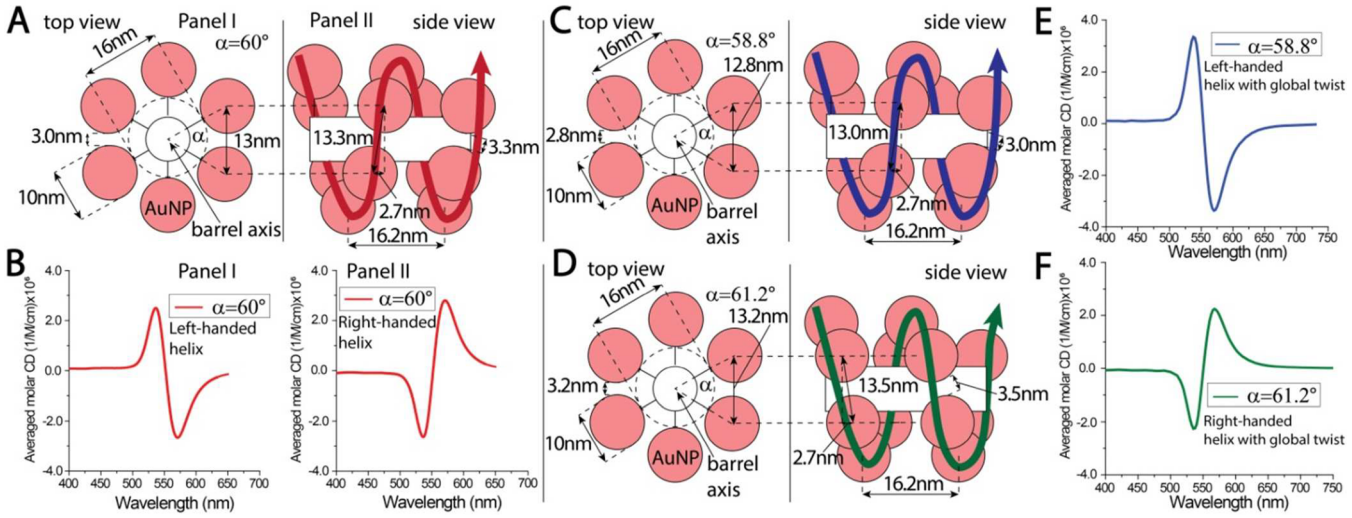

Figure 4. Theoretical simulations of the CD spectra of the left- and right-handed helical structures of the Au NPs associated with the barrels. (A) Schematic geometrical model for the Au NPs functionalizing the barrel: panel I, top view; panel II, side view. Angle α corresponds to the angle between two adjacent Au NPs and the axis of the barrel, $\alpha = 60°$. (B) Calculated CD spectra corresponding to the left-handed and right-handed helical structures of the plasmonic Au NPs (for details on the calculations, see Methods). (C) and (D) Geometrical paramters corresponding to the separation between the Au NPs in the left- and right-handed helices, taking into account the global right-handed twist in the DNA scaffolds. (E) and (F) Calculated CD spectra corresponding to the left-handed and right-handed helical configurations of the 12 Au NPs associated with the barrels subjected to the global right-handed twist, respectively.

DOI: 10.1021/jacs.6b04096
J. Am. Chem. Soc. 2016, 138, 9895−9901

across the diameter of the barrels is $d_1 = 16 \pm 3$ nm whereas the maximum distance between two Au NPs at the edges of the longitudinal axis of the barrel is $d_2 = 30 \pm 4$ nm. Accordingly, the top-view of the six Au NPs forming one rim of the helix is shown in Figure 4A, panel I, whereas Figure 4A, panel II, depicts the lateral view of the two full helices of Au NPs, associated with one side of the barrel. Knowing the values of d_1 and d_2, and using simple geometrical considerations, the distances between the respective particles were calculated as given in the two panels. The mirror image of the left-handed Au NPs structure given in Figure 4A is shown in Figure S15. Using these dimensions, the models of the left-handed and right-handed Au NP helices were constructed, Figure S16, and these allowed the Discrete Dipole Approximation (DDA) calculation of the (L)- or (R)-handed helical structures CD signals, Figure 4B. Evidently, the experimental patterns of the CD spectra are well reproduced and show the bisignate peak/dip bands centered around the plasmon absorbance band of the Au NPs presented in Figure 3. The calculated intensities of the CD bands for the (L)- and (R)-handed Au NPs assemblies are within the experimental range, yet reveal similar intensities. The higher CD bands observed for the (L)-handed helical Au NP configurations are rationalized in terms of torsional stress originating from local underwinding of the duplex DNA in the barrel structures.[49] In our design, we have 10.67 bp per turn (derived from the distance between consecutive crossover points) as compared to the theoretical 10.5 base-pairs/turn in B-DNA. This unbalanced torsional stress of ca. 2% is released by a global right-hand twist in the barrel structures (a similar unbalanced torsional stress leading to a global twist of an origami structure was previously addressed[49]). This global twist in the barrel structure is anticipated to increase the interparticle distances between adjacent Au NPs associated with the helical tethers of the same handedness as the global twist. In turn, this global twist in the barrel structure is anticipated to decrease the interparticle distances between adjacent Au NPs when associated with the helical tethers of the opposite handedness. That is, the 60° angle between consecutive particles is expected to increase to 61.2° in the (R)-handed configurations, and to decrease to 58.9° in the (L)-handed configurations. Figure 4C and D depicts the geometrical models for the (L)-handed and (R)-handed helical Au NP structures subjected to the (R)-handed global twist, respectively, and Figure 4E and F shows the relative calculated CD spectra. One may realize that the (L)-handed Au NP structure, subjected to the (R)-handed global twist, that results in an interparticle distance of 3.0 nm (vs 3.3 nm for the 60°) leads to CD bands that are ca. 30% intensified as compared to the calculated CD bands without the global twist. Similarly, one may realize that the (R)-handed helical Au NP assembly subjected to the (R)-handed global twist yields an interparticle distance of 3.5 nm (vs 3.3 nm for the 60°) that results in a decrease of ca. 50% in the intensities of the CD bands. That is, the intensities of the CD bands of the (L)-handed Au NPs are anticipated to be ca. 1.8-fold higher than the CD band intensities of the (R)-handed Au NPs, consistent with the experimental results.

It should be noted that the structural features of the 24-mer nucleic acid promoter units have a significant effect on the formation of the right/left-handed helical structures of the tethers and the resulting attached Au NPs: (i) We find that 15-mer tethers (T) alone, in the absence of promoter units (Ps), do not lead to any chiroselective formation of the tether-functionalized barrels or helical structure of the Au NPs. That is, although the tethers could provide steric/electrostatic repulsive interactions, the short chains of the free tethers and their positions on the barrel scaffold are insufficient to induce chiral assemblies. (ii) Short-chain 15-mer promoter units (Ps) are insufficient to yield Au NPs-functionalized barriers of noticeable CD responses. These results imply that promoter-driven chiroselective assembly of the barrels, and the formation of chiroplasmonic structures, require bulky long-chain promoter units. (iii) The hybridization of complementary nucleic acids to the long-chain promoter strands, PsC, did not improve the yield of the chiroplasmonic structures, cf. Figure S17. That is, despite the enhancing of the electrical repulsive interactions associated with the double-strand promoter units, the CD spectra of the chiroplasmonic structures are unchanged. These results might imply that the steric effects rather than the electrostatic repulsive interactions play a major role in the chiroselective formation of the plasmonic NP structures.

CONCLUSIONS

The present study has introduced a new paradigm to construct programmed tether-modified barrels for the organization of right- or left-handed chiral plasmonic Au NPs configurations. The folding of the barrels was dictated by "promoter" strands, Ps, that induced, by electronic and/or steric interactions, the assembly of right- or left-handed tethers for the deposition of the plasmonic chiral Au NP configurations. In this context, it is important to note that our approach relies on constant quasi-circular/stapled subunits modified identically by the tethers for the attachment of the Au NPs, and only the positioning of auxiliary promoter units drive the formation of the barrels with dictated chirality of the helicity of the tethers. The chiral plasmonic features of the different Au NP configurations were followed by CD spectroscopy and the results were supported by theoretical computations. Interestingly, the CD bands of the left-handed helical configurations of the Au NPs are intensified as compared to the CD bands of the right-handed helical configurations of the Au NPs. This phenomenon was attributed to a global twist of the DNA barrel scaffold.

The study introduced new concepts advancing the area of chiroplasmonic nanoparticle structures. The scalability of the assembly of the barrels into wires suggests that such helical nanoparticle architectures could be implemented as chiroplasmonic wave-guides.

METHODS

DNA Barrel Preparation and Characterization. The appropriate DNA sequences (Integrated DNA Technologies, details in the Supporting Information), 100 nM each, final volume 50 μL, were added to a solution containing 20 mM magnesium acetate and 0.5× TAE buffer (Tris-Acetate EDTA) and incubated in a thermal bath while decreasing the temperature from 90 to 60 °C within 20 min and from 60 to 4 °C within 14 h. The solution was then filtered using a Amicon 30 kDa MWCO at 10 000g for 5 min at 10 °C, using the buffer employed in the assembly of the barrels. AFM imaging was conducted in liquid, using the same buffer. A few microliters of the sample were deposited on freshly cleaved mica that subsequently was washed two times with buffer. The surface was then subjected to a buffer droplet while imaging the surface in the solution. Bruker ScanAsyst software was used with the appropriate ScanAsyst-Fluid$^+$ probe. DLS measurements were performed with a Malvern Zetasizer in a plastic cuvette in the same buffer used for the thermal bath incubation, taking care to filter all solutions with Whatman 0.22 μm filters before barrels assembly. Detailed protocols are reported in the Supporting Information.

DOI: 10.1021/jacs.6b04096
J. Am. Chem. Soc. 2016, 138, 9895−9901

Au NP Helices Assembly and Characterization, and CD Analysis. Commercial Au NPs 10 nm (BBI Solutions) were modified with thiolated DNA following an estabilizhed protocol.[50] The Au NPs were incubated overnight with an excess of bis(*p*-sulfonatophenyl)-phenylphosphine dihydrate dipotassium salt (BSPP) and filtered with an Amicon Ultra 100 kDa MWCO device at 5000*g* for 3 min, at room temperature, to eliminate the excess of the capping compound and concentrate the particles. After spectrophotometric determination of the Au NPs concentration, they were mixed in a 1:1 ratio with reduced thiol-modified DNA sequences T′ and sequences T″, that elongates the sequences T′ by partial complementarity, in a solution containing 100 mM NaCl, 0.5× TBE buffer (Tris Borate EDTA), 0.5 mg/mL BSPP and incubated for 3 h at room temperature. After gel electrophoresis separation in 3% agarose gel, the single-strand modified Au NP band was excided and the particles extracted in a dialysis tube. The collected particles were then incubated for 48 h in buffer with T″-releasing strand RT″ and a short thiolated DNA oligonucleotide Stab (HS-dT_5), prior to filtering using Amicon Ultra 100 kDA MWCO to eliminate the excess of HS-dT_5. To obtain the AuNP helices, 3 μL of the assembled barrel solution was mixed with the appropriate mix of T′-modified Au NPs, with a ratio 1:12, in a solution containing 20 mM magnesium acetate in 0.5XTAE buffer for 48 h at room temperature. The samples were then analyzed in a Jasco CD spectropolarimeter in a 1 cm light-path quartz cuvette and three signal accumulations for each experiment were averaged. TEM characterization of the Au NP assemblies was performed with HR-STEM Magellan (FEI). A few microliters of the Au NP-decorated barrels solution (1 nM) were deposited on a TEM copper mesh and freeze-dried prior to imaging.

Computational Modeling of the CD Spectra. We employed the Discrete Dipole Approximation method[51−53] (DDA) for our theoretical understanding of the measured CD signals obtained from left and right handed helical structures. The frequency dependent bulk permittivity of gold has been taken from the literature.[54] The dielectric constant of the medium is taken as 1.8 (water and DNAs) to account for the surrounding medium of the helical structures. In the optical experiments, the structures are randomly oriented in solution. Therefore, in order to calculate the CD signal, one is required to take the average of the CD for all possible directions of the incident left and right circularly polarized (LCP/RCP) lights on the structures. To reduce time-consuming computations while achieving accurate results, in the simulation, LCP and RCP beams are sent to the structure from three orthogonal directions. It was previously demonstrated that this approach is adequate to compute the features of small structures.[55] Accordingly, the extinction cross sections for circularly polarized photons are calculated. Subsequently, for each orthogonal direction, the CD signal is obtained by the difference between the LCP and RCP extinction cross sections. Finally, the averaged CD was computed by taking the average of the three directional CD signals. The input parameters for our optical plasmonic modes were the coordinates of NPs.

■ ASSOCIATED CONTENT

Supporting Information

The Supporting Information is available free of charge on the ACS Publications website at DOI: 10.1021/jacs.6b04096.

Sequences of different DNA strands; method to assemble the barrels; preparation and purification of single-nucleic acid functionalized Au NP; method to assemble the chiral plasmonic Au NP structure; HR-TEM images of the different chiroplasmonic structures; analysis of the Au NP barrels on large areas; statistical analysis of the yields of the different chiral structures; experimental and theoretical absorption spectra of different chiral Au NP structures and derived anisotropy *g*-factors; 3D model for the simulation of the CD spectra; superposition of the 2D projected 3D helical structure of the 12 Au NP functionalized structure on the 2D HR-TEM images (PDF)

■ AUTHOR INFORMATION

Corresponding Author

*willnea@vms.huji.ac.il

Notes

The authors declare no competing financial interest.

■ ACKNOWLEDGMENTS

This research is supported by the ERC Advanced Grant and by the Israel Science Foundation (I.W.). L.K.K. and A.O.G. are supported by the Volkswagen Foundation and by the US Army Research Office Grant W911NF-12-1-0407.

■ REFERENCES

(1) Ben-Moshe, A.; Maoz, B. M.; Govorov, A. O.; Markovich, G. *Chem. Soc. Rev.* **2013**, *42*, 7028.
(2) Guerrero-Martınez, A.; Alonso-Gomez, J. L.; Auguié, B.; Cid, M. M.; Liz-Marzan, L. M. *Nano Today* **2011**, *6*, 381.
(3) Tan, S. J.; Campolongo, M. J.; Luo, D.; Cheng, W. *Nat. Nanotechnol.* **2011**, *6*, 268.
(4) Guerrero-Martinez, A.; Auguié, B.; Alonso-Gómez, J. L.; Džolić, Z.; Gómez-Graña, S.; Žinić, M.; Cid, M. M.; Liz-Marzán, L. M. *Angew. Chem., Int. Ed.* **2011**, *50*, 5499.
(5) Xia, Y.; Zhou, Y.; Tang, Z. *Nanoscale* **2011**, *3*, 1374.
(6) Chen, W.; Bian, A.; Agarwal, A.; Liu, L.; Shen, H.; Wang, L.; Xu, C.; Kotov, N. A. *Nano Lett.* **2009**, *9*, 2153.
(7) Xia, Y. H.; Zhou, Y. L.; Tang, Z. Y. *Nanoscale* **2011**, *3*, 1374.
(8) Nie, Z.; Petukhova, A.; Kumacheva, E. *Nat. Nanotechnol.* **2010**, *5*, 15.
(9) Nakashima, T.; Kobayashi, Y.; Kawai, T. *J. Am. Chem. Soc.* **2009**, *131*, 10342.
(10) Elliott, S. D.; Moloney, M. P.; Gun'ko, Y. K. *Nano Lett.* **2008**, *8*, 2452.
(11) Li, Y. Y.; Zhou, Y. L.; Wang, H. Y.; Perrett, S.; Zhao, Y. L.; Tang, Z. Y.; Nie, G. J. *Angew. Chem., Int. Ed.* **2011**, *50*, 5860.
(12) Govan, J. E.; Jan, E.; Querejeta, A.; Kotov, N. A.; Gun'ko, Y. K. *Chem. Commun.* **2010**, *46*, 6072.
(13) Sanchez-Castillo, A.; Roman-Velazquez, C.; Noguez, C. *Phys. Rev. B: Condens. Matter Mater. Phys.* **2006**, *73*, 045401.
(14) George, J.; Thomas, K. G. *J. Am. Chem. Soc.* **2010**, *132*, 2502.
(15) Auguie, B.; Alonso-Gomez, J. L.; Guerrero-Martinez, A.; Liz-Marzan, L. M. *J. Phys. Chem. Lett.* **2011**, *2*, 846.
(16) Guo, X. M.; Jiang, C.; Shi, T. S. *Inorg. Chem.* **2007**, *46*, 4766.
(17) Zhu, M.; Qian, H.; Meng, X.; Jin, S.; Wu, Z.; Jin, R. *Nano Lett.* **2011**, *11*, 3963.
(18) Chen, Y.; Zeng, C.; Liu, C.; Kirschbaum, K.; Gayathri, C.; Gil, R. R.; Rosi, N. L.; Jin, R. *J. Am. Chem. Soc.* **2015**, *137*, 10076.
(19) Govorov, A. O.; Gun'ko, Y. K.; Slocik, J. M.; Gerard, V. A.; Fan, Z. Y.; Naik, R. R. *J. Mater. Chem.* **2011**, *21*, 16806.
(20) Gautier, C.; Burgi, T. *ChemPhysChem* **2009**, *10*, 483.
(21) Che, S.; Liu, Z.; Ohsuna, T.; Sakamoto, K.; Terasaki, O.; Tatsumi, T. *Nature* **2004**, *429*, 281.
(22) Wu, X.; Ruan, J.; Ohsuna, T.; Terasaki, O.; Che, S. *Chem. Mater.* **2007**, *19*, 1577.
(23) Shopsowitz, K. E.; Qi, H.; Hamad, W. Y.; MacLachlan, M. J. *Nature* **2010**, *468*, 422.
(24) Liu, S.; Han, L.; Duan, Y.; Asahina, S.; Terasaki, O.; Cao, Y.; Liu, B.; Ma, L.; Zhang, J.; Che, S. *Nat. Commun.* **2012**, *3*, 1215.
(25) Fan, Z.; Govorov, A. O. *Nano Lett.* **2012**, *12*, 3283.
(26) Chen, C.-L.; Zhang, P.; Rosi, N. L. *J. Am. Chem. Soc.* **2008**, *130*, 13555.
(27) Pazos, E.; Sleep, E.; Rubert Pérez, C. M.; Lee, S. S.; Tantakitti, F.; Stupp, S. I. *J. Am. Chem. Soc.* **2016**, *138*, 5507.
(28) Wang, F.; Lu, C.-H.; Willner, I. *Chem. Rev.* **2014**, *114*, 2881.
(29) Wilner, I. O.; Willner, I. *Chem. Rev.* **2012**, *112*, 2528.

DOI: 10.1021/jacs.6b04096
J. Am. Chem. Soc. 2016, 138, 9895−9901

(30) Mastroianni, A. J.; Claridge, S. A.; Alivisatos, A. P. *J. Am. Chem. Soc.* **2009**, *131*, 8455.
(31) Yan, W. J.; Xu, L.; Xu, C.; Ma, W.; Kuang, H.; Wang, L.; Kotov, N. A. *J. Am. Chem. Soc.* **2012**, *134*, 15114.
(32) Fu, J.; Liu, M.; Liu, Y.; Woodbury, N. W.; Yan, H. *J. Am. Chem. Soc.* **2012**, *134*, 5516.
(33) Fu, Y.; Zeng, D.; Chao, J.; Jin, Y.; Zhang, Z.; Liu, H.; Li, D.; Ma, H.; Huang, Q.; Gothelf, K. V.; Fan, C. *J. Am. Chem. Soc.* **2013**, *135*, 696.
(34) Lund, K.; Manzo, A. J.; Dabby, N.; Michelotti, N.; Johnson-Buck, A.; Nangreave, J.; Taylor, S.; Pei, R.; Stojanovic, M. N.; Walter, N. G.; Winfree, E.; Yan, H. *Nature* **2010**, *465*, 206.
(35) Kuzyk, A.; Schreiber, R.; Fan, Z.; Pardatscher, G.; Roller, E.-M.; Högele, A.; Simmel, F. C.; Govorov, A. O.; Liedl, T. *Nature* **2012**, *483*, 311.
(36) Shen, X.; Asenjo-Garcia, A.; Liu, Q.; Jiang, Q.; García de Abajo, F. J.; Liu, N.; Ding, B. *Nano Lett.* **2013**, *13*, 2128.
(37) Shen, X.; Zhan, P.; Kuzyk, A.; Liu, Q.; Asenjo-Garcia, A.; Zhang, H.; García de Abajo, F. J.; Govorov, A.; Ding, B.; Liu, N. *Nanoscale* **2014**, *6*, 2077.
(38) Kuzyk, A.; Schreiber, R.; Zhang, H.; Govorov, A. O.; Liedl, T.; Liu, N. *Nat. Mater.* **2014**, *13*, 862.
(39) Schreiber, R.; Luong, N.; Fan, Z.; Kuzyk, A.; Nickels, P. C.; Zhang, T.; Smith, D. M.; Yurke, B.; Kuang, W.; Govorov, A. O.; Liedl, T. *Nat. Commun.* **2013**, *4*, 2948.
(40) Urban, M. J.; Zhou, C.; Duan, X.; Liu, N. *Nano Lett.* **2015**, *15*, 8392.
(41) Ma, W.; Kuang, H.; Xu, L.; Ding, L.; Xu, C.; Wang, L.; Kotov, N. A. *Nat. Commun.* **2013**, *4*, 2689.
(42) Petersen, J.; Volz, J.; Rauschenbeutel, A. *Science* **2014**, *346*, 67.
(43) Söllner, I.; Mahmoodian, S.; Hansen, S. L.; Midolo, L.; Javadi, A.; Kiršanskė, G.; Pregnolato, T.; El-Ella, H.; Lee, H. H.; Song, J. D.; Stobbe, S.; Lodahl, P. *Nat. Nanotechnol.* **2015**, *10*, 775.
(44) Zheng, H.; Xiao, M.; Yan, Q.; Ma, Y.; Xiao, S.-J. *J. Am. Chem. Soc.* **2014**, *136*, 10194.
(45) Zhao, Y.; Xu, L.; Ma, W.; Wang, L.; Kuang, H.; Xu, C.; Kotov, N. A. *Nano Lett.* **2014**, *14*, 3908.
(46) Govorov, A. O.; Fan, Z. *ChemPhysChem* **2012**, *13*, 2551.
(47) Govorov, A. O. *J. Phys. Chem. C* **2011**, *115*, 7914.
(48) Abdulrahman, N. A.; Fan, Z.; Tonooka, T.; Kelly, S. M.; Gadegaard, N.; Hendry, E.; Govorov, A. O.; Kadodwala, M. *Nano Lett.* **2012**, *12*, 977.
(49) Ke, Y.; Douglas, S. M.; Liu, M.; Sharma, J.; Cheng, A.; Leung, A.; Liu, Y.; Shih, W. S.; Yan, H. *J. Am. Chem. Soc.* **2009**, *131*, 15903.
(50) Elbaz, J.; Cecconello, A.; Fan, Z.; Govorov, A. O.; Willner, I. *Nat. Commun.* **2013**, *4*, 2000.
(51) Draine, B. T.; Flatau, P. J. *J. Opt. Soc. Am. A* **1994**, *11*, 1491.
(52) Draine, B. T.; Flatau, P. J. *J. Opt. Soc. Am. A* **2008**, *25*, 2693.
(53) Flatau, P. J.; Draine, B. T. *Opt. Express* **2012**, *20*, 1247.
(54) Johnson, P. B.; Christy, R. W. *Phys. Rev. B* **1972**, *6*, 4370.
(55) Fan, Z.; Govorov, A. O. *Nano Lett.* **2012**, *12*, 3283.

DOI: 10.1021/jacs.6b04096
J. Am. Chem. Soc. 2016, 138, 9895−9901